Effects of pH on Rhodopsin Photointermediates from Lumirhodopsin to Metarhodopsin II[†]

Stefan Jäger, Istvan Szundi, James W. Lewis, Tina L. Mah, and David S. Kliger*

Department of Chemistry and Biochemistry, University of California, Santa Cruz, California 95064

Received November 18, 1997; Revised Manuscript Received January 22, 1998

ABSTRACT: Time-resolved absorption difference spectra of membrane suspensions of bovine rhodopsin at pH 5, 6, 7, 8, 9, and 10 were collected in the time range from 1 μs to 200 ms after laser photolysis with 7-ns pulses of 477-nm light. The data were analyzed using singular value decomposition (SVD) and global exponential fitting. At pH 7 the data agree well with previously obtained data (Thorgeirsson et al. (1993) *Biochemistry 32*, 13861−13872) with fits improved at all pH's by inclusion of a small component due to an absorbance change caused by rotational diffusion which is detectable even at magic angle polarization. A "square scheme" suggested to best explain the previous data, which involves two branches following decay of the lumi intermediate with pathways (1) lumi $\rightarrow$ MI_{480} $\rightleftharpoons$ MII and (2) lumi $\rightleftharpoons$ MI_{380} $\rightarrow$ MII, could be confirmed throughout the entire pH range. However, to account for the increased rate of the MII $\rightarrow$ MI_{480} reaction in path 1 for rising pH values, we propose that the MII in the square scheme consists of deprotonated MII* and protonated MII*H^+ forms in rapid equilibrium with each other, resulting in an extended square scheme and increasing the number of 380-nm products from two to three. In addition to the kinetic processes described by the extended square scheme, above pH 8 fast ($\sim$10 μs) and slow ($\sim$50 ms) components were found. The fast component was assigned to the decay of a blue-shifted lumi intermediate, and the slow component, resolvable only at pH 10, was assigned to formation of a 450 nm absorbing photoproduct.

Rhodopsin is a G protein coupled photoreceptor protein which initiates an enzyme cascade leading to visual transduction (*1*, *2*). The light-sensitive chromophore, 11-*cis*-retinal, is bound to Lys^{296} via a protonated Schiff base (PSB)[1] linkage. The counterion to the PSB has been identified as Glu^{113} (*3*−*5*). Light-induced cis−trans isomerization transforms the retinylidine chromophore into the all-trans configuration. This primary photochemical event triggers a cascade of photointermediates involving thermal transitions in the protein moiety. One way of characterizing the intermediates is by performing time-resolved absorption measurements to determine the microscopic rate constants for their interconversions and to determine their absorption maxima (*6*). The intermediate which directly interacts with the G protein to initiate the enzyme cascade leading to visual transduction is metarhodopsin-II (MII; *7*, *8*). Of particular interest is how this active MII state is formed.

Early work on photointermediates showed that the spectra of rhodopsin photoproducts are pH dependent (*9*−*12*). Scheme 1 describes the classic scheme for proton uptake:

Scheme 1

$$MI + nH^+ \rightleftharpoons MII \qquad 0.6 < n < 1.0$$

For the early photointermediates up to lumirhodopsin (lumi), the following scheme has been proposed (*13*):

Scheme 2

$$\text{rho} \xrightarrow{h\nu} \text{batho} \rightleftharpoons \text{bsi} \rightarrow \text{lumi} \rightarrow , \ldots$$

Spectra and kinetics of these intermediates have been shown to be insensitive to solvent conditions (*14*). The reaction scheme leading from lumi to MII is described most satisfactorily by the "square scheme" introduced in Thorgeirsson et al. (*15*):

Scheme 3

$$\begin{array}{ccc} \ldots \text{lumi} & \rightleftharpoons & MI_{380} \\ \downarrow & & \downarrow \\ MI_{480} & \rightleftharpoons & MII \end{array}$$

Here MI_{380} is a deprotonated Schiff base intermediate, distinct from MII, formed directly from lumi. To study rhodopsin's mechanism for MII formation, the pH (e.g., this study), the temperature (*15*), or the ionic strength (*16*) can be varied, or the system can be perturbed in other ways, e.g., by adding long-chain alcohols (*17*). All of these factors influence MII formation, but the general scheme which describes the transformations between the intermediates should be the same

[†] This work was supported by NIH Grant EY00983 to D.S.K.

* To whom correspondence may be addressed.

[1] Abbreviations: batho, bathorhodopsin; bsi, blue-shifted intermediate of rhodopsin; BTP, 1,3-bis[tris(hydroxymethyl)methylamino]propane; EDTA, ethylenediaminetetraacetic acid; FTIR, Fourier transform infrared; lumi, lumirhodopsin; MI, metarhodopsin I; MII, metarhodopsin II; MES, 2-(*N*-morpholino)ethanesulfonic acid; NMR, nuclear magnetic resonance; PIPES, 1,4-piperazinediethanesulfonic acid; PSB, protonated Schiff base; rho, rhodopsin; R*, light-activated rhodopsin; ROS, rod outer segment; SVD, singular value decomposition; WT, wild type.

S0006-2960(97)02819-5 CCC: $15.00
Published on Web 04/28/1998

for sufficiently small perturbations. We have thus used perturbation studies to test the viability of reaction Scheme 3.

The absorption spectrum of rhodopsin (λ_{max} = 500 nm) does not change between pH 6 and 9 (*18*), and the protonated Schiff base is not attacked by hydroxylamine in the dark. In a modeling study, using NMR constraints on the position of the counterion as well as data involving mutations on helices 3 and 6, it has been suggested that protein conformational changes leading up to Schiff base deprotonation are driven by steric interactions, while Schiff base deprotonation and subsequent changes are driven by electrostatic interactions (*19*). It thus seems plausible that the protein is affected by pH changes in the late (Scheme 3) rather than in the early (Scheme 2) intermediates.

Recently it was shown that proton uptake, as indicated by bromocresol purple, and Schiff base deprotonation (380-nm absorbance change) show different kinetics when the protein is solubilized in detergent. A two-step reaction was proposed (*20*):

Scheme 4

$$MI \rightleftharpoons MII_a \overset{+nH^+}{\rightleftharpoons} MII_b \qquad n = 2$$

In two mutant studies involving Glu^{134} it was shown that (1) Glu^{134} is involved in the proton uptake, mediating the uptake of *both* protons in the reaction $MII_a \rightleftharpoons MII_b$ (*21*), and (2) Glu^{134} in the protonated form favors the binding of R* to transducin (*22*). It should be noted that FTIR measurements have not shown the protonation reaction of Glu^{134}, possibly because Glu^{134} is only transiently protonated. In another mutant study it was shown that, in digitonin solutions, His^{211} is essential to reach MII and that neutral residues at positions His^{65} and His^{152} promote MII formation at alkaline pH compared to WT (*23*). This demonstrates that the proton reaction after photolysis of rhodopsin is more complicated than simply the titration of one group.

To date, pH-dependent kinetic measurements on rhodopsin have involved time-resolved optical measurements at single wavelengths, an approach unlikely to be effective for testing a complex mechanism like Scheme 3. In the present report we monitored absorbance difference spectra of membrane suspensions of bovine rhodopsin from pH 5 to 10 with microsecond time resolution using a pulsed probe source and multichannel detection. By using global exponential fitting of the time-dependent spectral data, we were able to deduce the kinetics and λ_{max} values of all intermediates in the pH range from pH 5 to 10. One goal of this study was to test whether Scheme 3 can explain time-resolved spectral data over a wide range of pH and whether this scheme can be interpreted in terms of the observations mentioned above. However, the broader goal is to elucidate the role of ionizable groups in the progression of rhodopsin photointermediates.

MATERIALS AND METHODS

Sample Preparation. Rhodopsin in native disk membrane was washed hypotonically (to eliminate peripheral proteins such as transducin) as described previously (*24*), with the exception that MES (pH 5 and 6) and BTP buffers (pH 7−10) were used instead of PIPES. The disk membranes were resuspended in the buffers containing 30 mM NaCl, 60 mM KCl, 2 mM $MgCl_2$, and 0.1 mM EDTA. The membrane suspensions were sonicated mildly to decrease light scattering. To avoid bubble formation in the measuring cuvette, the samples were degassed prior to measurements. The sample temperature was maintained at 20 °C using a copper insert connected to a water bath.

Time-Resolved Spectroscopy. All laser photolysis measurements were performed either in an apparatus which pumped individual 24-μL aliquots of sample before each photolysis pulse (*13*, *25*) or in a microapparatus using 1-μL aliquots (*26*). The data collected from the two different flow systems were the same after correction for the path length difference. The pigment solution was photolyzed by 7-ns (fwhm), 80 $\mu J/mm^2$ pulses of 477-nm light from a Quanta Ray DCR-2 Nd:YAG pumped dye laser. The laser beam entered the sample at an angle of 90° from the probe beam, with vertical polarization. The probe beam polarization axis was set at magic angle (54.7°) with respect to the laser beam polarization to avoid kinetic artifacts due to rotational diffusion. The probe beam path length through the sample was 10 mm for the macro- and 2 mm for the microapparatus. After each laser pulse, the sample was replaced by a flow system using a syringe whose plunger was controlled by a computer-driven stepper motor. Difference spectra were measured with a gated optical multichannel analyzer system as described previously (*25*, *27*).

Data Analysis. The data were analyzed using singular value decomposition (SVD) followed by a global exponential fitting procedure as described elsewhere (*13*, *15*, *28*). This procedure fits the absorbance difference spectra (e.g., Figure 1b, representing the average of four independent data sets at pH 7) at all wavelengths and delay times simultaneously. In the fitting procedure the best fit was taken to be the one with the smallest number of exponentials giving reasonable residuals (actual data minus fit; e.g., Figure 2b). The next step was to find a kinetic scheme which can account for the time constants, τ_i, and their corresponding eigenvectors, called b spectra (e.g., Figure 3b, solid curves). Once the kinetic scheme was chosen, it was translated into a kinetic matrix and fit to the τ_i's and b spectra (e.g., Figure 3b, dotted lines) using appropriate intermediate spectra. We were able to use the same set of λ_{max} values for all intermediate spectra. To verify the validity of the fit, the fitted kinetic matrix and the experimental b spectra were used to calculate the experimental intermediate − bleach spectra (e.g. Figure 4b, solid curves). The "bleach" consists of the spectrum of the rhodopsin bleached corrected for any isorhodopsin formed by each laser pulse and can be determined independently (*29*). The experimental intermediate − bleach spectra were finally compared to their theoretical counterparts to determine the quality of the fit (e.g., Figure 4b, dotted lines) (*30*).

RESULTS

Absorption difference spectra of membrane suspensions of bovine rhodopsin were collected at pH 5, 6, 7, 8, 9, and 10 (T = 20 °C). The data sets taken near physiological pH (6, 7, and 8) and at pH 10 are shown in Figure 1 and will be discussed in detail to demonstrate the general pH-dependent features which prevail near physiological pH and to point out new features which appear at alkaline pH's. The data at pH 5 and 9 fit into the trend of the pH dependence

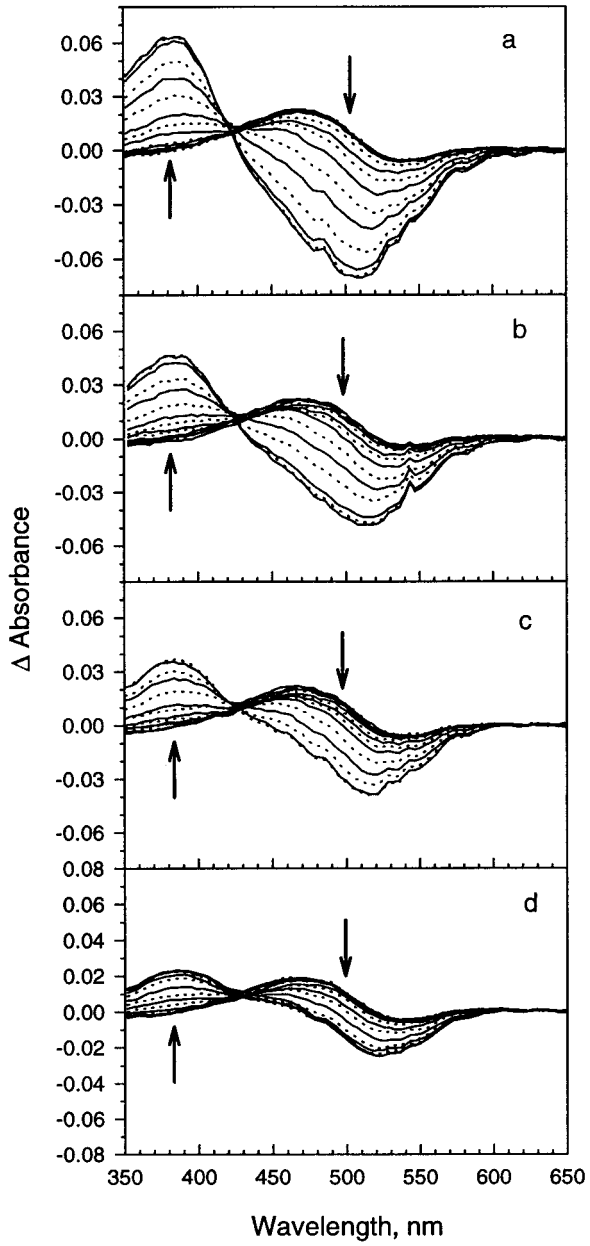

FIGURE 1: Difference spectra for rhodopsin in membrane suspensions after photolysis with 7-ns (fwhm) 477-nm laser pulses at 20 °C. Spectra were collected at 1, 2, 5, 10, 20, 50, 100, 200, 500 μs and 1, 2, 5, 10, 20, 50, 100, 200 ms after photolysis. Arrows indicating progression of spectra from early to late times are shown for pH 6, 7, 8, and 10, panels *a*, *b*, *c*, and *d*, respectively.

established at the other pH's (data not shown). Each data set represents the average of four independent measurements. Inspection of the 200-ms difference spectra clearly shows dependence on pH. Increasing the pH of the sample decreases the amount of the deprotonated ($\lambda_{max} \sim 380$ nm) and increases the amount of the protonated ($\lambda_{max} \sim 480$ nm) Schiff base forms of the final photoproducts, respectively. This anomalous pH dependence is known in the literature and shows that the protonation steps involve a scheme that is more complex than a simple chromophore protonation/deprotonation.

pH 7. Figure 1b shows the absorption difference spectra at pH 7 measured at times 1, 2, 5, 10, 20, 50, 100, 200, and 500 μs and 1, 2, 5, 10, 20, 50, 100, and 200 ms after photolysis. The data were analyzed using singular value decomposition (SVD) followed by a global exponential fitting procedure (Materials and Methods). In the 10-μs−200-ms time range a three-exponential fit to the absorption difference spectra with time constants $\tau_1 = 100$ μs, $\tau_2 = 1.9$ ms, and $\tau_3 = 20.9$ ms gives reasonable residuals, in good agreement with previous results (*15*, *17*). When additional data in the 1−10-μs time range are included in the analysis, the three-exponential fit can be improved by including an additional fast exponential, resulting in time constants $\tau_{fast} = 6$ μs, $\tau_1 = 120$ μs, $\tau_2 = 2.1$ ms, and $\tau_3 = 21.0$ ms, summarized in Table 1. The residuals of the four-exponential fit are shown in Figure 2b, and the difference spectra corresponding to the time constants, called b spectra, are presented in Figure 3b (solid curves). The b_{fast}, shown as a broken line, is not considered to be part of the main reaction path, and for reasons presented in the discussion it is believed to come from a rotational diffusion artifact. Therefore only b_1, b_2, b_3, and b_0 are included in the determination of the reaction scheme. For consistent interpretation of pH-dependent reaction rate changes, the fast component lifetime at all pH's measured was fixed at the 6-μs value corresponding to rotational relaxation.

Table 1: Summary of the Apparent Time Constants[a] Corresponding to the b Spectra of Membrane Suspensions of Bovine Rhodopsin Measured from pH 5 to 10

	pH					
lifetime	5	6	7	8	9	10
τ_{fast}	6.0 μs	6.0 μs	6.0 μs	6.0 μs	6.0 μs	6.0 μs
τ_1 (±20 μs)	135 μs	140 μs	120 μs	130 μs	115 μs	120 μs
τ_2 (±0.15 ms)	0.9 ms	1.4 ms	2.1 ms	2.3 ms	1.4 ms	1.4 ms
τ_3 (±1 ms)	9.40 ms	16.3 ms	21.0 ms	13.4 ms	7.6 ms	6.8 ms
τ_{slow}	N/A	N/A	N/A	N/A	N/A	60.0 ms

[a] The estimated uncertainties of the time constants are given, except for τ_{fast} which was fixed at the 6-μs value appropriate for rotational diffusion (see text).

The elements of the kinetic scheme can be deduced from the b spectra (*28*). The b_1 spectrum represents the lumi to MI_{380} transition. Its small amplitude suggests a back-shifted equilibrium step. The b_2 spectrum shows the simultaneous transition of lumi to MI_{480} and MII, indicating a branching at the lumi state. The b_3 spectrum represents the MI_{480} to MII transition. The b_0 spectrum shows the final composition minus the bleach. Addition of the photolyzed rhodopsin spectrum to b_0 reveals the presence of some MI_{480} in addition to the dominant MII species in the final product. As expected, the square scheme (Scheme 3) was able to fit the b spectra (Figure 3b, dotted lines) and their corresponding time constants satisfactorily. Table 2 summarizes the microscopic time constants resulting from the fit. They were used, together with the b spectra, to calculate the intermediate − bleach spectra for lumi, MI_{380}, MI_{480}, and MII (Figure 4b). Experience with the fitting procedure has shown that this last step is a sensitive and hence a useful one for fine-tuning the fitting process. In Figure 5b the concentration profile calculated from the kinetic matrix is shown. The final intermediates are MI_{480} and MII, which are in equilibrium with each other (Scheme 3). The pathway lumi $\rightarrow$ $MI_{480} \rightleftharpoons$ MII is the traditional pathway deduced from low-temperature trapping studies, but it represents only one of two possibilities leading to the active MII state. MI_{380} is an early transient state, with a deprotonated Schiff base, which is in a fast

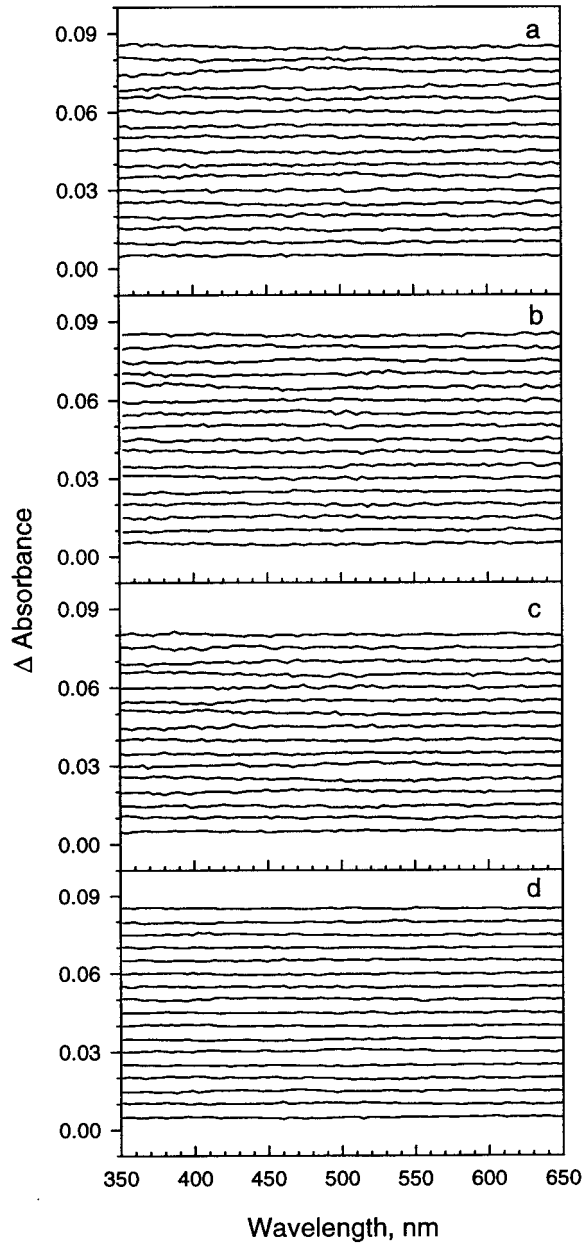

FIGURE 2: Residuals representing the actual data minus multiexponential fit for pH 6, 7, 8, and 10, panels *a*, *b*, *c*, and *d*, respectively. The 1-μs residual is shown at the bottom of each panel.

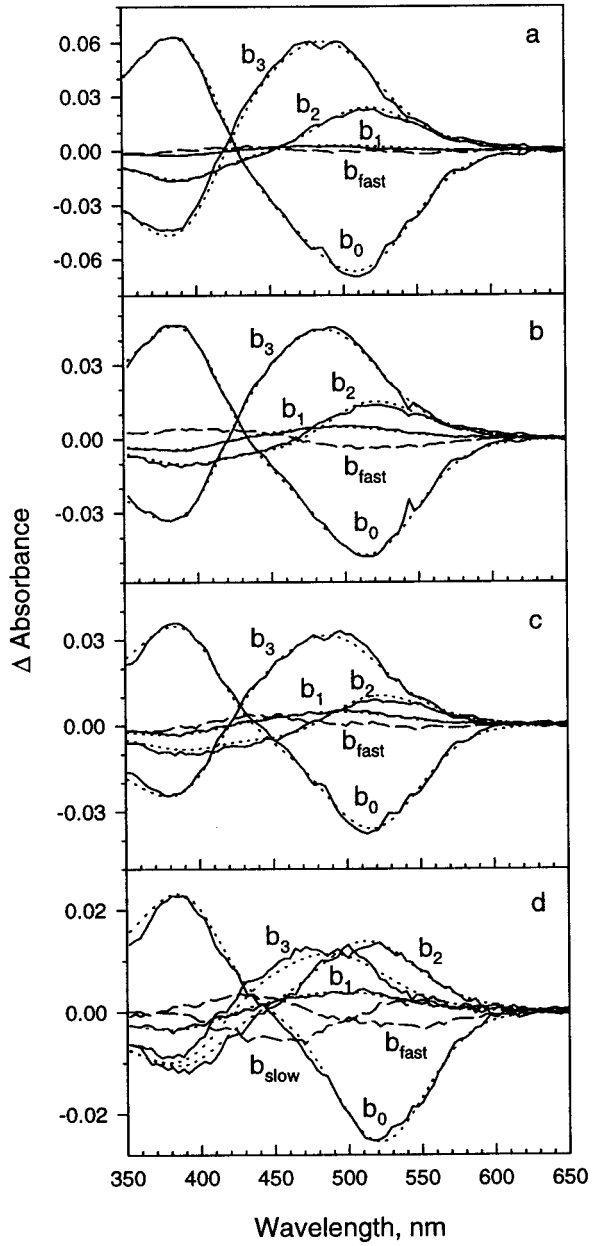

FIGURE 3: b spectra which resulted from multiexponential fits of data (solid curves) and as deduced from the fitting process using Scheme 3 (dotted curves) for pH 6, 7, 8, and 10, panels *a*, *b*, *c*, and *d*, respectively. The b spectra shown in broken lines were not used for the determination of the scheme (see text).

equilibrium with lumi and decays with a time constant of ~600 μs to MII. This pathway provides the second way to reach the active MII state. Both equilibrium constants, lumi $\rightleftharpoons$ MI_{380} (K_1) and MI_{480} $\rightleftharpoons$ MII (K_2), are given in Table 2.

pH 6. Figure 1a shows the absorption difference spectra for pH 6 measured at the same times after photolysis as for pH 7. A three-exponential fit reproduced the data in the 10-μs−200-ms time range. However, again, the fit in the entire time range could be improved by introducing an additional fast component with $\tau_{fast} = 6$ μs. The remaining time constants are shown in Table 1, and the corresponding b spectra are shown in Figure 3a. Omitting the fast process, the τ_i's and b spectra could be fit to Scheme 3, resulting in microscopic time constants of the intermediates which are summarized in Table 2. Figure 4a shows the intermediate − bleach spectra resulting from the fit to Scheme 3. Compared to pH 7, the equilibrium constant K_1 increased only slightly (by a factor of 1.3), whereas K_2 increased by a factor of 4. The concentration profile of the intermediates, shown in Figure 5a, shows that the MI_{480} $\rightleftharpoons$ MII equilibrium is shifted toward MII. The kinetics of MII production is slightly faster at pH 6.

pH 8. Absorption difference spectra for pH 8 (Figure 1c) were collected under identical conditions and at the same times as for pH 6 and 7. In the 10-μs−200-ms time range, three exponentials were sufficient to fit the data, and with the early time points included, a four-exponential fit again gave better residuals. Figure 3c shows the four-exponential fit with time constants given in Table 1. The most striking difference relative to lower pH's is the shape of b_0 (the time-independent difference spectrum), which shows smaller amplitude at 380 nm (deprotonated form) and a positive contribution at 480 nm (protonated form). Omitting the fast component, b_{fast}, enables Scheme 3 to fit the b spectra (dotted

Table 2: Summary of the Microscopic Time Constants of the Intermediates of Membrane Suspensions of Bovine Rhodopsin from pH 5 to 10

	pH					
species	5	6	7	8	9	10
lumi → MI_{380} (±20%)	1.1 ms	2.4 ms	1.8 ms	1.9 ms	1.6 ms	1.5 ms
MI_{380} → lumi (±15%)	400 μs	290 μs	160 μs	170 μs	170 μs	190 μs
lumi → MI_{480} (±10%)	1.7 ms	1.8 ms	2.6 ms	2.7 ms	1.7 ms	1.8 ms
MI_{380} → MII (±20%)	220 μs	290 μs	620 μs	740 μs	440 μs	720 μs
MI_{480} → MII (±10%)	9.7 ms	18 ms	30 ms	25 ms	15 ms	16 ms
MII → MI_{480} (±10%)	330 ms[a]	170 ms[b]	69 ms	28 ms	16 ms	12 ms
K_1 (±20%) (lumi ⇌ MI_{380})	0.37	0.12	0.091	0.091	0.10	0.13
K_2 (±15%) (MI_{480} ⇌ MII)	34[a]	9.1[b]	2.3	1.1	1.0	0.75

[a] Due to the large value of the equilibrium constant, this value has a larger estimated uncertainty (±50%). [b] Due to the large value of the equilibrium constant, this value has a larger estimated uncertainty (±30%).

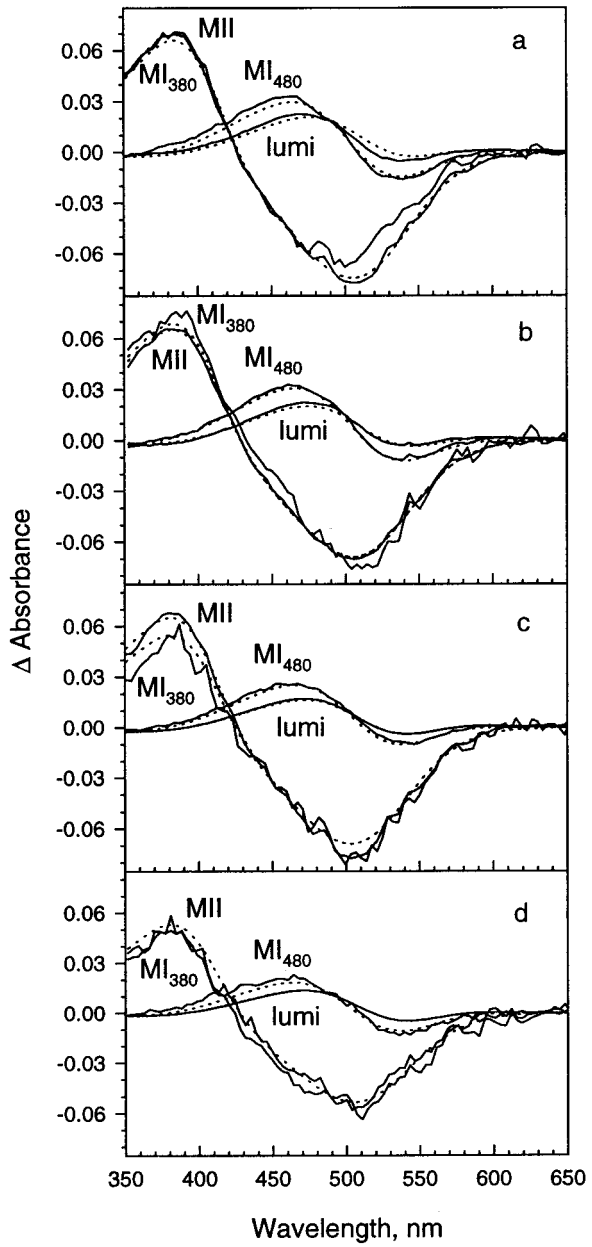

FIGURE 4: Intermediate minus bleach spectra (solid curves) calculated from the b spectra (Figure 3, solid curves) and the microscopic decay constants for pH 6, 7, 8, and 10, panels *a*, *b*, *c*, and *d*, respectively. The fits (dotted curves) represent the Gaussian shape of the intermediate − bleach spectra. The decay constants resulting from the fits are summarized in Table 2.

lines in Figure 3c). τ_1, τ_2, and τ_3 are in the range expected for the processes described by the square scheme at pH 6−8. The main difference between pH 6, 7, and 8 is the MI_{480} ⇌ MII equilibrium (K_2), which shifts to the MII side at pH 6 and reaches roughly equal MI_{480} and MII concentrations at pH 8. The lumi ⇌ MI_{380} equilibrium is back-shifted at all pH's, and hence makes only a small contribution to the signal we measure. Within the signal-to-noise limits, K_1 does not show a strong pH dependence in the physiological range.

pH 10. Figure 1d shows pH 10 absorption difference spectra collected under identical conditions and at the same times as for pH 6−8. Three- and four-exponential fits to the data did not give satisfactory residuals, so a fifth exponential (b_{slow}) was introduced. Figure 3d shows the b spectra with b_{fast} and b_{slow} plotted as broken lines. The corresponding τ's are given in Table 1. Like b_{fast}, b_{slow} is considered to be a process independent of the Scheme 3 framework and will be discussed later. As such, these processes were excluded from the determination of the main scheme presented here. Because b_{fast} and b_{slow} were omitted from the set of b spectra, b_0 no longer represents the final products of the reaction scheme. To calculate the correct b_0, we took advantage of the fact that the sum of all b spectra used in the fitting procedure (b_0, b_1, b_2, and b_3) should equal the absorption difference spectrum at the initial time of the reaction sequence, which was 1 μs in these experiments. Thus b_0 = (difference spectrum at 1 μs) − (b_1 + b_2 + b_3). The actual measured difference spectrum at 1 μs cannot be used in this calculation because it contains additional components that are not part of the reaction scheme treated here (see discussion). For this scheme (Scheme 3) the difference spectrum at 1 μs should be a pure lumi − bleach spectrum, which can be calculated from the rhodopsin and lumi model spectra with appropriate amplitudes. The corrected b_0 (in combination with b_1, b_2, and b_3) was then used to fit Scheme 3.

The relative contributions of the components b_2 and b_3 differ considerably from those deduced for pH 6−8. The amplitude of b_2 has increased at the expense of b_3, which now is smaller in amplitude than b_2. Scheme 3 was fit to b_1, b_2, b_3, and the corrected b_0. The fit is shown in Figure 3d, and the resulting microscopic time constants are given in Table 2. Figure 4d shows the intermediate − bleach spectra following from the fit to Scheme 3, and Figure 5d shows the concentration profile of the intermediates. It is obvious that the MI_{480} ⇌ MII equilibrium is back-shifted at pH 10.

pH 9. Absorption difference spectra for pH 9 (data not shown), measured at the same times as for the other pHs, were fit with four exponentials (see Table 1). After

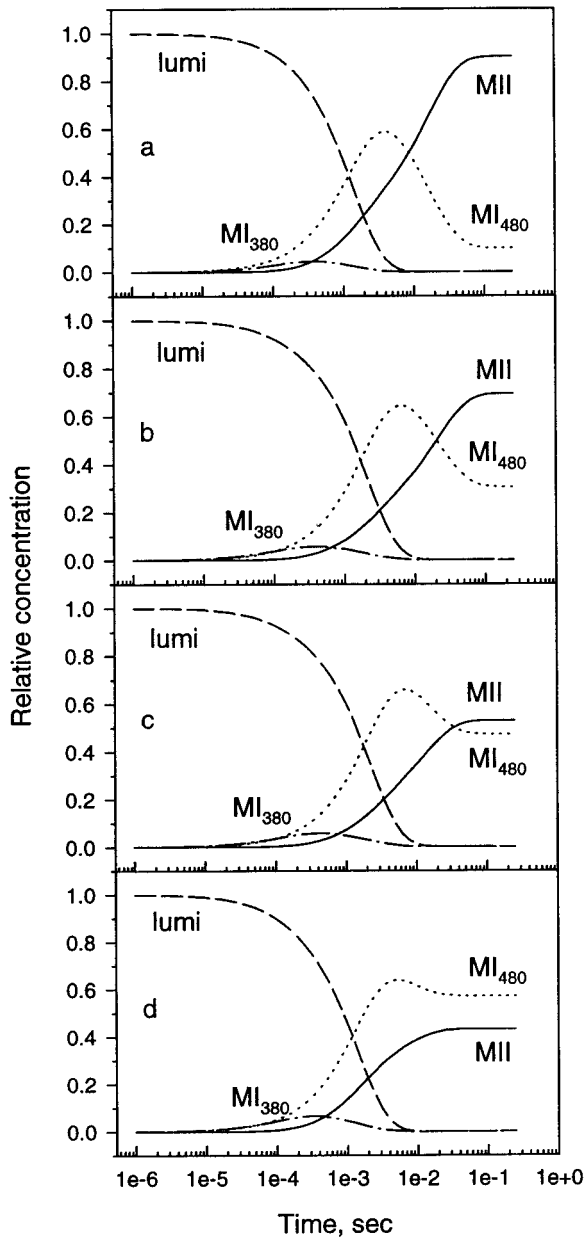

FIGURE 5: Concentration profiles of the intermediates as a function of time for pH 6, 7, 8, and 10, panels *a*, *b*, *c*, and *d*, respectively.

excluding b_{fast}, an attempt was made to fit the b spectra to Scheme 3 using the same set of intermediate spectra that gave satisfactory fits at the other pH values. However, the fit was poor, with the agreement between the fit and the experimental b_3 spectrum being particularly unsatisfactory. Decomposing the b spectra using the intermediate spectra revealed that besides the expected components, MI_{480} and MII, b_3 had an additional component similar to the b_{slow} detected at pH 10. This suggested that a slow component might be hidden in b_3, the slowest component of the four-exponential fit of the pH 9 data. After correction of b_0 and b_3 by attributing a 0.6 fraction to b_{slow}, we were able to fit the τ's and the b spectra to Scheme 3. The microscopic time constants and equilibrium constants are given in Table 2.

pH 5. Absorption difference spectra for pH 5 were measured at the same times as for pH 6−10 (data not shown). The analysis of the data set was the same as for pH 6−8. The three-exponential fit was improved by introducing a fast component with time constants shown in Table 1. The shapes of the b spectra, however, differ from those deduced for pH 6−8: b_2 has increased at the expense of b_3, as observed for pH 10, but the amplitude of b_3 is still somewhat larger than that of b_2 (data not shown). The τ_i and b spectra again could be fit to Scheme 3, with time constants given in Table 2.

DISCUSSION

In this study we performed kinetic analysis of absorption difference spectra from bovine rhodopsin measured in the time window corresponding to the lumi-to-MII transformation, varying the pH from 5 to 10 in membrane suspensions. These data can be used to determine the relationship between the early 380 nm absorbing intermediate and the multiple 380 nm absorbing forms proposed to exist at later times (*7*, *31*). The previously reported early deprotonated photoproduct, denoted as MI_{380} (*15*, *17*), was observed at all pH's, and over the pH 5−8 range the reaction mechanism originally proposed to fit the temperature-dependent data at pH 7, Scheme 3, was able to fit the photochemical decays observed. Besides the components described by Scheme 3, an additional fast component with associated spectral change b_{fast} was detected at all pH's. For pH < 9, b_{fast} is very small compared to the other b spectra and is not accompanied by a component corresponding to the b_{slow} observed at pH 9 and 10. Further, b_{fast} has the difference spectrum associated with rotational relaxation of a photoselected rhodopsin/lumirhodopsin mixture in the disk membrane (*32*) and has approximately the same time dependence observed there. Even though we collected our data at magic angle polarization, it seems likely that b_{fast} at the low pH's results from a polarization artifact. The way such an artifact can arise is that light-scattering-induced beam deviations break down the assumed cylindrical symmetry around the laser's vertically polarized electric vector. Careful measurements of $A_{||}$ and $A_{\perp}$ at pH 7 do indeed find the implied light-scattering-induced photolysis bias for molecules with transition dipole moments in the vertical plane, which contains the laser's propagation direction, compared to the vertical plane containing the probe beam propagation direction (data not shown). To correct the kinetic data for the polarization artifact consistently at each pH, the lifetime of the fast component was fixed at 6 μs, the time constant of rotational relaxation. At pH 10, the presence of b_{slow} and differences in the shape of b_{fast} indicate a more complex origin, which we interpret in terms of an additional chemical process besides those described by Scheme 3. Given that near physiological pH only the reactions described by the standard square scheme manifest themselves, we interpret those reactions first.

In the square scheme there exist two pathways to the active MII state: the traditional pathway, lumi $\rightarrow$ MI_{480} $\rightleftharpoons$ MII, and the pathway via the early deprotonated form (MI_{380}), lumi $\rightleftharpoons$ MI_{380} $\rightarrow$ MII. Inspection of Table 2 shows that in the physiological pH range the equilibrium constant for MII formation (K_2) is much more strongly pH dependent than is the equilibrium constant for MI_{380} formation (K_1), making the fast equilibrium relatively pH independent. As a consequence, the behavior of MI_{380} in the square scheme cannot account for the anomalous pH dependence of the observed MII formation rate. This anomaly consists of the

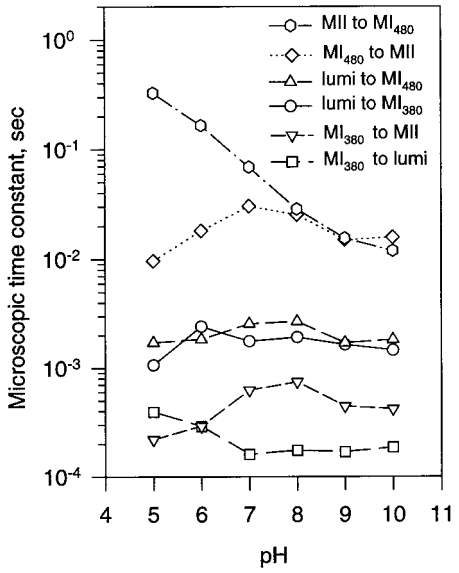

FIGURE 6: pH dependence of the microscopic rates in Scheme 3.

fact that while a simple MI + nH$^+$ ⇌ MII might be expected to slow as the pH increases from 7 to 8, the observed rate of 380 nm absorbance growth appears to increase over this range (*12*, *16*, *31*, *33*). Even with MI_{380} in the scheme, the microscopic rates in Table 2 associated with MII formation continue to show apparent base catalysis (see Figure 6). In particular, the back rate from MII to MI_{480} shows a pronounced increase with pH.

A natural way to account for the kinetics observed here is to assume that the MII in the square scheme actually consists of deprotonated MII* and protonated MII*H$^+$ forms in rapid equilibrium with each other, as shown below:

Scheme 5

$$\begin{array}{ccc} \text{... lumi} & \rightleftharpoons & MI_{380} \\ \downarrow & & \downarrow \\ MI_{480} & \rightleftharpoons & \text{MII*} \overset{H^+}{\rightleftharpoons} \text{MII*H}^+ \end{array}$$

Then under the assumption that the only form of MII which decays to MI_{480} is MII*, the slowing of the apparent MII → MI_{480} back rate becomes a mass action consequence of the reduced MII* population in the MII* ⇌ MII*H$^+$ equilibrium mixture. For such an extended scheme to be consistent with the finding of three observed rates, all that is required is that the MII* ⇌ MII*H$^+$ equilibrium be rapid, a property to be expected for protonation of an exposed group by solvent.

A similar proton equilibrium between two MII forms has been proposed for bovine (*31*) and frog (*33*) rhodopsins, but those models involving only two MII forms, neither formed directly from lumi, are unable to fit observations on bovine rhodopsin suspensions at physiological temperatures (*15*), so an additional 380 nm absorbing form is required in addition to the two MII pH forms. Besides explaining the apparent base catalysis, the presence of two MII forms also accounts for the difficulty encountered in completely titrating MII away at higher temperatures and the less than unity slope of the pH titration curve (*11*, *12*). From our K_2 data, the pK associated with titration of the MII* ⇌ MII*H$^+$ equilibrium is near 7. The associated amino acid side chain could thus be a histidine titrated at the more acidic pH prevailing at the membrane compared to the bulk pH.

The involvement of His^{211} in the bovine MI_{480} ⇌ MII equilibrium has been indicated by site-directed mutagenesis (*23*), and further support for the importance of this sequence position comes from measurements on the cone-type visual pigment P521 from the lizard *Gekko gekko*. There the slowest (and potentially largest) component of MII formation was titrated with a pH of 8.7, which the authors concluded was a consequence of a cysteine (solution pK 8.7) occupying the sequence position equivalent to bovine His^{211} (*34*). Other work has indicated that His^{211} is not essential for the activity of bovine rhodopsin toward transducin (*35*). However, this does not preclude an important role for His^{211} in MII formation since transducin activation experiments are influenced not only by MII formation but also by MII decay, and hence cannot be interpreted solely in terms of MII formation.

In addition to intermediates previously described by the square scheme, we found that two other processes, b_{fast} and b_{slow}, were needed to adequately describe our data. For low pH's the dominant component of b_{fast} was assigned to rotational diffusion, whereas for high pH values (pH 9 and 10) an additional chemical process besides those described by the standard square scheme was implicated. This raises the question of where the b_{fast} component, measured at pH 9 and 10, comes from. Decomposing the first difference spectrum measured at 1 μs (pH 9 or 10) shows that it does not solely consist of a pure lumi − bleach spectrum. To look for additional intermediates which might already be present together with the known early intermediates (e.g., batho to lumi), we measured absorption difference spectra at pH 9 from 30 ns to 200 ms (data not shown). The data analysis showed that, up to lumi, Scheme 2 does not change and confirmed the additional component b_{fast} with a time constant τ_{fast} of 10−30 μs. On this time scale a new intermediate, absorbing around 450 nm, decays to a product absorbing to the red of rhodopsin. The question arises, does this red intermediate decay, and where does the product of this decay appear in the spectrum? At pH 10 there exists a slow exponential component, b_{slow}, which seems to account for this process. The fact that b_3 from the pH 9 data set had to be corrected with b_{slow} (deduced from pH 10) shows that such an exponential component is also present at pH 9 with a smaller time constant. The nature of the new intermediate is not clear. One possibility is that a fraction of the lumi intermediate has shifted to the blue, because a titratable group with pK_a around 10 has been deprotonated. This group is not the Schiff base, Lys^{296}, because the new intermediate absorbs around 450 nm in the deprotonated form. Titration of a peripheral group to produce a blue-shifted alkaline lumi could explain why it is so difficult to extract this additional process kinetically. Presumably such a group would be relatively loosely coupled to the activation mechanism, resulting in a new component which would decay with time constants which do not differ significantly compared to normal lumi, and hence such processes would be difficult to separate kinetically. Since a blue-shift of rhodopsin under extreme conditions (high pH, 4 M KCl) with a pK of 10.2 has been reported (*18*), it is reasonable to assume that wavelength shifts under extreme pH conditions are manifested in the intermediates as well. Such a process may account for a pK near 9 which has been identified for base inhibition of rhodopsin's activity toward transducin (*35*).

Even near neutral pH where fewer processes occur, the pH data reported here show surprising complexity. The presence of three distinct deprotonated Schiff base intermediates has made data collection and even nomenclature difficult. This complexity certainly accounts for the large number of attempts which have been made to characterize the reactions described here. An additional complication is the sensitivity of the late photointermediates to the protein environment. Previously, in detergent-solubilized rhodopsin it has been proposed that deprotonation of the Schiff base and proton uptake by the receptor occur in two consecutive reactions, with proton uptake being mandatory to reach the active state (*20*). Arnis and Hofmann calculated an apparent pK_a of 6.75 from their titration curve of that proton-uptake reaction. Detailed comparison of their spectroscopic results (*20*) with ours requires reconciliation of the different schemes involved (two 380 nm intermediates there versus three here). Because the kinetics is faster in detergent suspensions than it is in membrane, it is more difficult to resolve the decay components. However, array detectors and modern matrix methods allow progress to be made even on such complex systems. Preliminary results show that Scheme 5 also prevails in detergent suspensions of rhodopsin, and further, in that system proton uptake in the MII* $\rightleftharpoons$ MII*H^+ reaction can be directly observed in the absorbance changes of a pH-sensitive dye (Mah et al., manuscript in preparation). The data presented here provide the critical link between those detergent results and the behavior of rhodopsin in the membrane environment which exists in vivo.

REFERENCES

1. Stryer, L. (1986) *Annu. Rev. Neurosci. 9*, 87−119.
2. Stryer, L. (1991) *J. Biol. Chem. 266*, 10711−10714.
3. Sakmar, T. P., Franke, R. R., and Khorana, H. G. (1989) *Proc. Natl. Acad. Sci. U.S.A. 86*, 8309−8313.
4. Zhukovsky, E. A., and Oprian, D. D. (1989) *Science 246*, 928−930.
5. Nathans, J. (1990) *Biochemistry 29*, 9746−9752.
6. Kliger, D. S., and Lewis, J. W. (1995) *Isr. J. Chem. 35*, 289−307.
7. Hofmann, K. P. (1986) *Photobiochem. Photobiophys. 13*, 309−338.
8. Hofmann, K. P., Jäger, S., and Ernst, O. P. (1995) *Isr. J. Chem. 35*, 339−355.
9. Lythgoe, R. J. (1937) *J. Physiol. 89*, 331−358.
10. Wald, G. (1938) *J. Gen. Physiol. 21*, 795−832.
11. Matthews, R. G., Hubbard, R., Brown., P. K., and Wald, G. (1963) *J. Gen. Physiol. 47*, 215−240.
12. Parkes, J. H., and Liebman, P. (1984) *Biochemistry 23*, 5054−5061.
13. Hug, S. J., Lewis, J. W., Einterz, C. M., Thorgeirsson, T. E., and Kliger, D. S. (1990) *Biochemistry 29*, 1475−1485.
14. Lewis, J. W., Einterz, C. M., Hug, S. J., and Kliger, D. S. (1989) *Biophys. J. 56*, 1101−1111.
15. Thorgeirsson, T. E., Lewis, J. W., Wallace-Williams, S. E., and Kliger, D. S. (1993) *Biochemistry 32*, 13861−13872.
16. DeLange, F., Merkx, M., Bovee-Geurts, P. H. M., Pistorius, A. M. A., and DeGrip, W. J. (1997) *Eur. J. Biochem. 243*, 174−180.
17. Mah, T. L., Szundi, I., Lewis, J. W., Jäger, S., and Kliger, D. S. (1998) *Photochem. Photobiol.* (submitted).
18. Koutalos, Y. (1992) *Biophys. J. 61*, 272−275.
19. Shieh, T., Han, M., Sakmar, T. P., and Smith, S. O. (1997) *J. Mol. Biol. 269*, 373−384.
20. Arnis, S., and Hofmann, K. P. (1993) *Proc. Natl. Acad. Sci. U.S.A. 90*, 7849−7853.
21. Arnis, S., Fahmy, K., Hofmann, K. P., and Sakmar, T. P. (1994) *Biochemistry 33*, 23879−23881.
22. Fahmy, K., and Sakmar, T. P. (1993) *Biochemistry 32*, 7229−7236.
23. Weitz, C. J., and Nathans, J. (1992) *Neuron 8*, 465−472.
24. Thorgeirsson, T. E., Lewis, J. W., Wallace-Williams, S. E., and Kliger, D. S. (1992) *Photochem. Photobiol. 56*, 1135−1144.
25. Lewis, J. W., Warner, J., Einterz, C. M., and Kliger, D. S. (1987) *Rev. Sci. Instrum. 58*, 945−949.
26. Lewis, J. W., and Kliger, D. S. (1993) *Rev. Sci. Instrum. 64*, 2828−2833.
27. Einterz, C. M., Lewis, J. W., and Kliger, D. S. (1987) *Proc. Natl. Acad. Sci. U.S.A. 84*, 3699−3703.
28. Szundi, I., Lewis, J. W., and Kliger, D. S. (1997) *Biophys. J. 73*, 688−702.
29. Albeck, A., Friedman, N., Ottolenghi, M., Sheves, M., Einterz, C. M., Hug, S. J., Lewis, J. W., and Kliger, D. S. (1989) *Biophys. J. 55*, 233−241.
30. Jäger, S., Lewis, J. W., Zvyaga, T. A., Szundi, I., Sakmar, T. P., and Kliger, D. S. (1997) *Biochemistry 36*, 1999−2009.
31. Emrich, H. E., and Reich, R. (1974) *Z. Naturforsch. Teil C 29*, 577−591.
32. Cone, R. A. (1972) *Nature New Biol. 236*, 39−43.
33. Baumann, C., and Zeppenfeld, W. (1981) *J. Physiol. 317*, 347−364.
34. Liang, J., Govindjee, R., and Ebrey, T. G. (1993) *Biochemistry 32*, 14187−14193.
35. Cohen, G. B., Oprian, D. D., and Robinson, P. R. (1993) *Biochemistry 31*, 12592−12601.

BI9728194